

New Study on the 1941 Gloria Fault Earthquake and Tsunami

Maria Ana Baptista^{1,2}, Jorge Miguel Miranda^{2,3}, Josep Batlló⁴, Filipe Lisboa³, Joaquim Luis^{2,5}, Ramon Maciá⁶

5 1 Instituto Superior de Engenharia de Lisboa, Instituto Politécnico de Lisboa, Lisboa, Portugal

2 Instituto Dom Luiz, Universidade de Lisboa, Lisboa, Portugal

3 Instituto Português do Mar e da Atmosfera, Lisboa, Portugal

4 Institut Cartogràfic i Geològic de Catalunya, Barcelona, Spain

5 Universidade do Algarve, Faro, Portugal

10 6 Dept. de Matemàtiques, Universitat Politècnica de Catalunya, Barcelona, Spain

Correspondence to: Maria Ana Baptista (mavbaptista@gmail.com)

Abstract. The M_w 8.3-8.4 25th November 1941 was one of the largest submarine strike-slip earthquakes ever recorded in the North East (NE) Atlantic basin. This event occurred along the Eurasia-Nubia plate boundary between the Azores and the Strait of Gibraltar. After the earthquake, the tide stations in the NE Atlantic recorded a small tsunami with maximum amplitudes of 40 cm peak to trough in Azores and Madeira islands. In this study, we present a re-evaluation of the earthquake epicentre location using seismological data not included in previous studies. We invert the tsunami travel times to obtain a preliminary tsunami source location using a backward ray tracing (BRT) technique. We invert the tsunami waveforms to infer the initial sea surface displacement using Empirical Green Functions without prior assumptions on the geometry of the source. The results of the BRT simulation locate the tsunami source quite close to the new epicentre. This fact suggests that the co-seismic deformation of the earthquake induced the tsunami. The waveform inversion of tsunami data favours the conclusion that the earthquake ruptured approximately 160 km segment of the plate boundary, in the eastern section of the Gloria Fault between -20.249°E and -18.630°E. The results presented here contribute to the evaluation of tsunami hazard in the North East Atlantic basin

1. Introduction

30 The western segment of the Eurasian-Nubian plate boundary extends from Mid-Atlantic Ridge in the Azores towards the Strait of Gibraltar. Between -24°E and -20°E, the plate boundary is supposed to follow a prominent morphological feature, the Gloria Fault firstly mapped by Laughton et al. (1972) (see figure 1 for location). The development of Gloria Fault as a segment of the Eurasia-Nubia plate boundary occurred ~27Myr ago (Luis and Miranda, 2008). The relative interplate motion is slow ~ 5 mm/year (Fernandes et al., 2003) with unusual seismic activity. In spite of this, a few large earthquakes have been located close to this plate boundary. The predominant focal mechanism is strike-slip (Buforn et al., 1998, 2004; Argus et al., 1989). Among these events, are the 25th November 1941 (Udias et al., 1976, Lynnes and Ruff, 1985),

the 9th June 1969 (Argus et al., 1989), and the 26th May 1975 (Buforn et al., 1988; Argus et al., 1989; Kaabouben et al., 2008) and the 17th October 1983 (Argus et al., 1989). Some of these earthquakes
40 generated tsunamis, described in historical documents and recorded by the tide stations, namely 31st March 1761, the 25th November 1941 and the 26th May 1975 (Baptista et al., 2006; Kaabouben et al., 2008; Baptista and Miranda, 2009).

In this study, we present a re-analysis of the seismic data of the 25 November 1941 event and the first
45 comprehensive analysis of the associated tsunami. We use a newly acquired set of historic seismograms to re-evaluate the position of the epicenter and the computation of the seismic moment. We digitized, de-tided and filtered all tide records available in the North East Atlantic basin. The use of seismic and tsunami data provides a better understanding of this earthquake and tsunami.

2. The 25th November 1941 Earthquake

50 The 25th November 1941 earthquake occurred at 18:03:54 (TUC). Madeira, Azores and western Portugal recorded the strongest shaking – VI (MSK). The earthquake impacted the neighboring countries: Spain and Morocco. The studies by Debrach (1946), Di Filippo (1949) and Moreira (1968) present macroseismic data analyses.

Antunes (1944) presented the first epicenter location, using only data from the Portuguese seismic network,
55 at -18.9°E, 38.7°N. Gutenberg and Richter (1949) relocated the epicenter at -18.5°E, 37.50°N and computed the earthquake magnitude as Ms=8.2. Later, Lynnes and Ruff (1985) using a master-event technique relative to a better characterized event (26th May 1975) relocated the epicenter at -19.1°E, 37.6°N. Udias et al. (1976) computed the earthquake magnitude as 8.3.

In this study, we present a relocation of the earthquake source using the phases published by the ISC bulletin
60 complemented with readings from nearby stations AVE in Morocco (-7.413³⁰E, 33.2961⁰N), FBR in Spain (2.123⁰E, 41.41840N) and MAL in Spain (-4.4292⁰E, 36.762⁰N). To compute the hypocenter, we used “Hypocenter”, a damped least square algorithm for earthquake location (Lienert et al., 1986), running under SEISAN environment, a seismic analysis package containing a complete set of programs and a simple database for analyzing earthquake data (Ottemöller et al., 2011).

65 Additionally, we tested two velocity models to compute the epicenter. The IASPEI91 velocity model (Kennett et al., 1991) locates the epicenter at -18.965⁰E, 37.344⁰N. The regional velocity model by Carrilho et al. (2004) for the Portuguese area locates the epicenter at -19.038⁰E, 37.405⁰N, which is our preferred solution. The focal depths given by these models are 12km (rms=2.5s) and 5.3km (rms=2.2s) respectively.

We computed the scalar seismic moment using the (Dineva et al., 2002) approach. Original analogue
70 seismograms were digitized and the seismic moment is computed from the spectra of body waves ground motion independently for each component. Twenty-six seismograms from fourteen seismic stations were digitized. Using P waves from thirteen stations we obtain a seismic moment of 3.96 10²¹ Nm, while using S waves from seven stations the seismic moment gives 2.96 x10²¹ Nm. These seismic moment values correspond to a moment magnitude of 8.3±0.2 and 8.2±0.3 respectively . To re-evaluate the focal
75 mechanism, we used the polarities from seventy-two seismograms. The parameters of the focal mechanism

are strike 76° , dip 88° and rake angle -161° . The focal mechanism is depicted in figure 1 and an example of a newly digitized seismogram is shown in figure 2.

3. Tsunami data analysis

80 After the earthquake, the tide stations in Portugal mainland, Morocco, Madeira and Azores Islands (see figure 1 for locations) recorded a small tsunami. In UK, Newlyn (-5.5°E , 50.1°N) tide station (not shown in figure 1) recorded the tsunami. Ponta Delgada tide station, in the Azores, recorded the maximum amplitude of 0.2 m. The Portuguese press reported tsunami observations close to Lisbon, and the overtopping of shallow areas close to Oporto (Leixões) (see Baptista and Miranda, 2009 for details). Haslett and Bryant
85 (2008) describe tsunami observations along the English Channel at Newlyn (Cornwall, United Kingdom) and Le Havre (France). Debrach (1946) and Rothé (1951) report damage to the submarine cables Brest–Casablanca and Brest–Dakar. In Spain, the Bulletin of the Seismic Observatory in Almeria reports tsunami observations wave in the Canary Islands but the tide record of Tenerife is unreadable.

In this study, we selected the records of seven tide stations presented in Table I. We digitized the original
90 paper records except those of Casablanca and Essaouira (Morocco). Debrach (1946) presents drawings of these tide-records: Casablanca-Petite Darse, Casablanca-Jetee-Transversale and Essaouira. We could not find the original records of these stations. Instead, we had to rely on the drawings reproduced in Debrach (1946). We discarded the station Casablanca-Petite-Darse because the position of the tide gauge is uncertain. In this study, we use Casablanca-Jetee-Transversale, here named Casablanca. We did not use the
95 record of Newlyn because of the quality of the record.

All digitized records were linearly interpolated into a one-minute time step. For de-tiding, we used a least squares algorithm to fit the interpolated data into polynomials whose degrees guaranteed an adjusted R-square parameter above 0.995. To further ensure the goodness of our de-tiding we applied a band-pass filter. The parameters of the filter are: end of the first stop band at 91 min, beginning of first pass-band at
100 89 min, end of the pass-band at 5 min and beginning of the second stop band at 2 min. The filter's magnitude response is of 30 dB attenuation in the first stop-band, a pass-band ripple of 1dB and a second stop-band attenuation of 40 dB. We used Morlet's continuous wavelet analysis. Wavelet analysis has the advantage of providing information when a particular wave component is present, even if it appears only once in the time series. Hence, it can be better suited to the analysis of transient signals like tsunami waves. In this
105 study, we present the results of wavelet analysis (equation 1), using the Morlet mother function (equation 2):

$$W_{\Psi|f}(a, b) = \int_{-\infty}^{+\infty} \frac{1}{\sqrt{a}} \Psi^* \left(\frac{t-b}{a} \right) f(t) \partial t \quad a, b \in \mathcal{R}, a > 0 \quad (1)$$

The Morlet mother function is given by a plane wave modulated by a Gaussian:

$$\Psi_0(\eta) = \pi^{-1/4} e^{i\omega_0\eta} e^{-\eta^2/2} \quad (2)$$

110 Where ω_0 is the non-dimensional frequency, here taken to be 6 to satisfy the admissibility condition.

Figure 3 depicts the tsunami signals and the results of wavelet analysis. Madeira station presents the smallest dominant period close to 6 minutes. Ponta Delgada, Cascais and Lagos present a dominant period

close to 12 minutes. Leixões presents a dominant period close to 20 minutes but this period is present in the spectrum well before the arrival of the tsunami - in this station the signal to noise ratio is low, when compared with the other records. Casablanca presents a 22.5 minute dominant period. In the case of Essaouira, the dominant period is 45 minutes.

4. Preliminary location of the tsunami source

We used the travel time of the first wave arrival at each station to compute a preliminary location of the tsunami source. To do this, we used the Backward Ray Tracing (BRT) technique (Gjevik et al., 1997). We defined a set of points of interest (POIs) one per tide station. The position of each POI is the grid node closest to the actual location of the tide station, at a depth not less than 10 meters to avoid strong non-linear effects. Table I shows the location and depth of POIs used in this study. We back propagated the wave fronts from each POI using the algorithm implemented in the Mirone suite (Luis, 2007). The location of the tsunami source is the minimum of the averaged travel time square errors (in the least squares sense). The spatial distribution of the misfit is given by:

$$\varepsilon^2(x, y) = \frac{\sum_{i=1}^n (t_i^o - t_i^p)^2}{n} \quad (3)$$

where t_i^o and t_i^p are the observed and predicted travel time for each POI and n is the total number of POIs.

To compute the BRT solution, we used the tsunami travel times shown in Table 1 and a bathymetric grid with a horizontal resolution of 0.1° . In figure 4, we present the minimum of the averaged travel time error, $\varepsilon(x, y) = 7.2$ minutes at -19.0°E , 37.35°N . This location is 10 km to the SE of the seismic epicenter - 19.038°E , 37.405°N , presented in section 2 (see figure 4).

The BRT method has limitations inherent to the linear shallow water approximation implying an overestimation of the speed in shallow waters. Nevertheless, in the case of the 1941 tsunami, the good azimuthal coverage ensures that these limitations are partially averaged out.

4. Tsunami waveform inversion

4.1 Inversion methodology

To estimate the initial sea surface displacement (tsunami source) we need to invert the tsunami waveforms. Moreover, for tsunamis generated by earthquakes, we assume that the initial sea surface displacement mimics the elastic deformation of the seafloor thus providing information on the earthquake focal mechanism.

The problem of tsunami waveform inversion without assuming a fault model was firstly addressed by Aida (1972, in Satake, 1987). Since then, many studies focused on the use of waveform inversion methods to estimate the tsunami source. These studies can be broadly divided in two categories: with a priori assumptions on the fault model (e.g. Satake, 1987 and 1993; Hirata et al. 2003; Titov et al. 2005), and without a priori assumptions on the the source namely Baba et al. (2005), Satake et al. (2005), Tsushima et al. (2009), Wu and Ho (2011), and Yasuda and Mase (2013).

Here, we use the method proposed by Tsushima et al. (2009), Koike et al. (2011) and Miranda et al. (2014) based on the use of Empirical Green Functions to efficiently perform the linear shallow water forward problem, where the synthesis of the tsunami waveform $\eta_m(t_t)$ at the m point of interest along the coast for the time span t_t is given by a superposition principle:

$$\eta_m(t_t) = \sum_{i=1}^{nl} \sum_{j=1}^{nc} G_{ij}^m(t_t) h_{ij} \quad (4)$$

where $(nl \times nc)$ are the set of unit sources and h_{ij} is the amplitude of the initial water displacement attributed to the ij unit source. $G_{ij}^m(t_t)$ is the response to the unitary source of the i th element of the sea surface at the j th location and m is the total number of unitary sources. The waveform inversion is simply obtained by solving:

$$\begin{bmatrix} G_{11}^1(t_1) & G_{12}^1(t_1) & G_{13}^1(t_1) & \dots & G_{nl\ nc}^1(t_1) \\ \dots & \dots & \dots & \dots & \dots \\ G_{11}^1(t_t) & G_{12}^1(t_t) & G_{13}^1(t_t) & \dots & G_{nl\ nc}^1(t_t) \\ \dots & \dots & \dots & \dots & \dots \\ G_{nl\ nc}^m(t_1) & G_{12}^m(t_1) & G_{13}^m(t_1) & \dots & G_{nl\ nc}^m(t_1) \\ \dots & \dots & \dots & \dots & \dots \\ G_{nl\ nc}^m(t_t) & G_{12}^m(t_t) & G_{13}^m(t_t) & \dots & G_{nl\ nc}^m(t_t) \end{bmatrix} \begin{bmatrix} h_{11} \\ h_{12} \\ h_{13} \\ \dots \\ h_{nl\ nc} \end{bmatrix} = \begin{bmatrix} \eta_1(t_1) \\ \dots \\ \eta_1(t_t) \\ \dots \\ \eta_m(t_1) \\ \dots \\ \eta_m(t_t) \end{bmatrix} \quad (5)$$

We incorporate the suggestion by Tsushima et al. (2009) defining an influence area around the minimum of the BRT. The initial water displacement is forced to become null as the distance to the minimum increases, therefore allowing the computation of a spatially compact solution. To do this, we added to (5) additional equations of the form:

$$[0 \ 0 \ 0 \ 0 \ \dots \ q \ \dots \ 0] \begin{bmatrix} h_{11} \\ h_{12} \\ h_{13} \\ \dots \\ h_{nl\ nc} \end{bmatrix} = [0] \quad (6)$$

where q is a positive number given by:

$$q(r) = 10 * \left(\frac{r}{r_{max}} - 1 \right) \quad (7)$$

and $r > r_{max}$ is the distance between each parameter (unit source) and the minimum of BRT. r_{max} is a cut-off distance after which the initial water displacement converges to zero. Equations (5) and (6) form a mixed-determined linear inversion problem (Menke, 2012) which can be solved in the sense of the least squares weighted minimum norm, by;

$$h^{est} = [G^T W_e G + p^2 D^T D]^{-1} G^T W_e \eta \quad (8)$$

In equation (8), D is the first order derivative operator, W_e is a diagonal matrix that weights the likelihood that we attribute to the different observations. Each observation corresponds to a single measurement made by a tide gauge. Different values of p correspond to various levels of smoothness of the final solution.

4.2 Application to the 25 November 1941 event

In this work, the study area is shown in figures 1 and 3, which limits are $-26.28^{\circ}E$ to $-5.020^{\circ}E$ and $31.08^{\circ}N$ to $42.65^{\circ}N$. The Green Functions Database covers the area defined by $-22.5^{\circ}E$ to $-17.4^{\circ}E$ and $35.5^{\circ}N$ to

38.6⁰N. This area has a total of 51 x 31 unit prisms. The dimensions of the unitary prisms are approximately 0.12° x 0.12°. The time span for the calculation was fixed as 180 min, and the time step as 1 min.

180 Experience shows that giving the same weight to all data points is misleading as later arriving waves carry information resulting from reflections and interference, which are very hard to simulate with the inversion procedure. Here, we used a simple strategy of attributing a larger weight to the first incoming wave. We used only two different weights (eq. 8) for the data set. Data between the origin time of the earthquake and the first tsunami wave weighted 100 times more than the remaining data values, except for the Essaouira
185 data.

Using the results of the BRT, we selected the area within the 10-minute contour (corresponding to an average travel time error of less than 10 minutes) as the influence area (see figure 4). We performed several tests to assess the best choice of the parameters (p , r_{max}) that describe the relative quality of the data, the smoothness in the final solution and the size of the influence area, respectively. Parameter p is non-
190 dimensional while r is measured in grid units, and corrected for the latitude.

In figure 5, we show a “chessboard” synthetic source, with alternating +1m/-1m displacements, to study the resolving power of the inversion procedure. The test reproduces the geometry of the inversion procedure (same location of the POIs, and identical values of p , and r_{max}). The results presented in figure 4 show that the inversion algorithm recovers most of the “chessboard” information inside the influence area. Different
195 values of r_{max} do not change qualitatively the results for the inner area. Nevertheless, the value of p must be tuned by “trial and error” to get the best trade-off between resolution and smoothness of the solution. The geometry of the tide gauge network, with no stations SW of the source area, decreases the resolution of the solution in that direction and increases the sensitivity towards changes in the smoothness parameter p .

200 Figure 6 shows the solutions for the same set of parameters used in the “chessboard” test. In all cases the maxima of the initial displacement field correspond to segment BC (see figure 4), matching the 10-minute error contour of the BRT and the earthquake epicentre. The lateral extent of the source is roughly 160 km.

Figure 7 depicts the comparison between the forward computation using the initial displacement field depicted in figure 6 for the preferred solution ($p=0.3$, $r=8$) and the observed data.

205

5. Discussion and Conclusions

The seismological data of the 25th November 1941 earthquake lead to an epicentre location at -19.038⁰E, 37.4050N, and a moment magnitude of 8.3. The new epicentre lies west of the epicentre presented by Gutenberg and Richter (1949). However, it is important to note that both determinations lie along segment
210 BC (see figure 4) of the plate boundary whereas Udias et al. (1976) and Antunes (1944) locate the epicentre further north.

The analysis of the tsunami data shows a clear signal of small amplitude in most of the stations with an apparent change in the frequency content except for Leixões. The spectral analysis of the tsunami records shows different frequency contents. These differences are mainly caused by differences in local
215 morphological conditions and to the relative position of the station and the seismic source. Madeira station

located approximately across strike shows the smallest dominant period of 6 minutes. Leixões, located along strike, shows the largest dominant period of 20 minutes. Ponta Delgada, Cascais and Lagos show dominant periods close to 11 minutes (see figures 1 and 3). These results are consistent with a tsunami source located along the Nubia-Eurasia plate boundary.

220 The BRT simulation locate the minimum of the averaged travel time (7.2 minutes), at -19.000E, 37.350N quite close to the epicentre location. This result is consistent with the fact that the earthquake's co-seismic deformation induced the tsunami. It also shows the coherence of the tsunami dataset.

225 Because of the limitations inherent to the use of the linear shallow water approximation and the location of the tide gauges inside the harbours we opted to give different weight to the data points corresponding to up the first incoming wave. The set of solutions shown in figure 6, corresponding to different values of p (smoothness) and r_{max} (influence area), show a similar deformation pattern. All solutions show a smooth profile with a maximum upward displacement of +0.6 m compatible with the initial sea surface displacement computed with Okada (1985) formulae for the co-seismic deformation due to a fault in an elastic half-space (see figure 6a). Moreover, all inverse-problem solutions favour the conclusion that the earthquake ruptured approximately 160 km of the plate boundary between -20.249°E and -18.630°E.

230 The results presented in figure 7 show that the inversion technique used here can fairly reproduce the first incoming wave for most of the observations presented in Table 1. In Cascais, the synthetic wave arrives eight minutes earlier than the observed wave. The location of the tide station inside the old harbour in a very shallow area (less than 4 m) might be responsible for this discrepancy. Also, the smoothness coefficient used to compute the inverse solution may contribute to "spread" the lateral extent of the source thus producing earlier arrivals at some points on the coast. The observation in Essaouira is incompatible with all solutions presented in figure 6. The lack of the original tide records of Morocco and the poor quality of their reproduction in Debrach (1946) does not allow for further investigation. However, we can not exclude the hypothesis of a local second tsunami source close to the coast of Morocco. Debrach (1946) and Rothé
235 (1951) report damages to the submarine cables Brest-Casablanca and Brest-Dakar after the earthquake. This fact may suggest the occurrence of a submarine landslide close to the coast of Morocco.

In spite of the limitations inherent to the use of old instrumental records, some of them with a low-amplitude signal to noise ratio, the inversion of the tsunami waveforms provides an independent estimate of the extension of the tsunami source and indirectly, the extent of the seismic source.

245 The seismic source solution (strike 76°, rake 161°) also favours the conclusion that the earthquake ruptured segment BC (see figure 4) of the plate boundary. This position coincides with a segment of the plate boundary that is marked by a change in strike when compared to the Gloria Fault between -23.960°E and -20.249°E (AB in figure 4), and to the eastern segment CD (see figure 4) between -18.142°E and -15.972°E. While the relative motion between Eurasia and Nubia generates pure strike slip events along AB and CD,
250 there is a significant thrust component associated with the seismic rupture within segment BC. This is consistent with both (seismic and tsunami) studies. Segments AB and CD follow the small circle of the Eurasia Nubia rotation pole while segment BC makes an angle of approximately 12° with the small circle of Nuvel 1A.

255 Due to the small Eurasia-Nubia relative motion in this segment of the plate boundary (5 mm/yr), the recurrence of similar events is long. However, other parts of the same plate boundary can generate similar

events, with noticeable effects in the North Atlantic coasts, and the tsunamigenic potential of the Gloria fault is relevant for the quantification of tsunami hazard in the North East Atlantic basin.

6. Acknowledgements

260 This work received funding from ASTARTE project Assessment Strategy and Risk Reduction for Tsunamis in Europe – Grant 603839 FP7. The authors wish to thank the fruitful discussions with Nuno Lourenço about the geology of the Gloria fault and the reviewers for their suggestions to improve this paper. The authors also thank Direção Geral do Território for making available data of Cascais and Lagos, Portugal. Copies of the paper tide records can be obtained from the authors.

265

References

Antunes, M.T.: Notas Acerca do Sismo de 25 de Novembro de 1941. 4th Congress of Portuguese Association for the Advance of Sciences, Porto, 18-24 June, 1942. Tomo III, 2nd Section, p. 161-172 (in Portuguese), 1944.

270

Argus, D. F., Richard G. Gordon, Charles DeMets, and Stein, S.: Closure of the Africa-Eurasia-North America plate motion circuit and tectonics of the Gloria fault. *J. Geophys. Res.*, Vol. 94, No. B5, Pages 5585–5602, doi: 10.1029/JB094iB05p05585, 1989.

275

Baba, T., Cummins, R., and Takane, H.: Compound fault rupture during the 2004 off the Kii Peninsula earthquake (M 7.4) inferred from highly resolved coseismic sea-surface deformation. *Earth, planets and space* 57.3, 167-172, doi: 10.1186/BF00351810, 2005.

Baptista, M. A., Miranda, P. M. A., Miranda, J. M., and Victor, L. M.: Constrains on the source of the 1755 Lisbon tsunami inferred from numerical modelling of historical data on the source of the 1755 Lisbon tsunami. *J. of Geodyn.*, 25(1), 159-174, doi:10.1016/S0264-3707(97)00020-3, 1998.

280

Baptista, M. A., Miranda, J. M., and Luis, J. F.: In search of the 31 March 1761 earthquake and tsunami source. *Bull. of the Seism. Soc. of America*, 96(2), 713-721, doi: 10.1785/0120050111, 2006.

Baptista, M. A., and Miranda, J.M.: Revision of the Portuguese catalog of tsunamis. *Nat. Hazards and Earth Syst. Sci.*, 9 (1), 25-42, doi:10.5194/nhess-9-25-2009, 2009.

285

Bufo E., Udias A., and Colombas M.: Seismicity, source mechanisms and tectonics of the Azores – Gibraltar plate-boundary. *Tectonophysics*, 152, 89-118, doi:10.1016/0040-1951(88)90031-5, 1998.

Bufo E., Bezzeghoud, M., Udias, A., and Pro, C.: Seismic sources on the Iberia-African plate boundary and their tectonic implications. *Pure and Appl. Geophys.*, 161(3), 623-646, doi:10/1007/s00024-003-2466-1, 2004.

290

Carrilho, F., Nunes, J.C., Pena, J., and Senos, M.L.: Catálogo Sísmico de Portugal Continental e Região Adjacente para o período 1970-2000, Instituto de Meteorologia, ISBN 972-9083-12-6, 2004.

- Debrach, J.: Raz de marée d'origine sismique enregistré sur le littoral atlantique du Maroc (in French). Service de Physique du Globe et de l'institut scientifique Chérifien, Annales, Maroc, 1946.
- DeMets, C., Gordon, R.G., and Argus, F.D.: Geologically current plate motions. *Geophys. J. Int.* (2010) 181, 1–80, doi: 10.1111/j.1365-246X.2009.04491.x, 2010.
- 295 Di Filippo, D. : Il terremoto delle Azzore del 25 Nov. 1941, *Annali Geofis.*, 2, 400-405, 1949.
- Dineva, S., Batlló, J., Mihaylov, D., and Van Eck, T.: Source parameters of four strong earthquakes in Bulgaria and Portugal at the beginning of the 20th century. *J. of Seism.*, 6(1), 99-123, doi: 10.123/A:1014249814998, 2002.
- Fernandes, R. M. S., Ambrosius, B. A. C., Noomen, R., Bastos, L., Wortel, M. J. R., Spakman, W., and
300 Govers, R.: The relative motion between Africa and Eurasia as derived from ITRF2000 and GPS data. *Geophys. Res. Lett.*, 30(16), doi: 10.1029/2003GL017089, 2003.
- Gjevik, B., Pedersen, G., Dybesland, E., Harbitz, C. B., Miranda, P. M. A., Baptista, M. A., P. Heinrich, R. Roche, M. Guesmia: Modeling tsunamis from earthquake sources near Goringe Bank southwest of Portugal. *Journal of Geophysical Research: Oceans*, 102(C13), 27931-27949, doi : 10.1029/97JC02179,
305 1979.
- Gutenberg, B., and Richter, C.F. *Seismicity of the earth and associated phenomena.* 273 pp. Princeton University Press, 1949.
- Haslett, S. K., and Bryant, E. A.: Historic tsunamis in Britain since AD 1000: a review. *Nat. Hazards Earth Syst. Sci.*, 8, 587-601, dx.doi.org/10.5194/nhess-8-587-2008, 2008.
- 310 Hayashi, Y., H., Tsushima, K., Hirata, Kimura, K., and Maeda, K.: Tsunami source area of the 2011 off the Pacific Coast of Tohoku earthquake determined from tsunami arrival times at offshore observation stations, *Earth Planets Space*, 63, 809–813, 10.5047/eps.2011.06.042, 2011.
- Hirata, K., Geist, E., Satake, K., Tanioka, Y., and Yamaki, S.: Slip distribution of the 1952 Tokachi- Oki earthquake (M 8.1) along the Kuril trench deduced from tsunami waveform inversion. *Journal of
315 Geophysical Research: Solid Earth* (1978–2012), 108(B4), doi: 10.1029/2002JB001976, 2003.
- Kaabouben, F., Brahim, A. I., Toto, E., Baptista, M. A., Miranda, J. M., Soares, P., and Luis, J. F.: On the focal mechanism of the 26.05. 1975 North Atlantic event contribution from tsunami modeling. *Journal of seismology*, 12(4), 575-583, doi: 10.1007/s10950-008-9110-6, 2008.
- Kennett, B.L.N., and Engdahl, E.R.: Travel times for global earthquake location and phase identification.
320 *Geophys. J. Int.*, 105, 429–465, doi: 10.1111/j.1365-246X.1991.tb06724.x, 1991.
- Koike, N.: Estimation of Tsunami Initial Displacement of Water Surface Using Inversion Method with a priori Information. INTECH Open Access Publisher, 2011.
- Laughton, A.S., Whitmarsh, R.B., Rusby, J.S.M., Somers, M.L., Revie, J., McCartney, B.S., and Nafe, J.E.: A Continuous East-West Fault on the Azores-Gibraltar Ridge. *Nature* 237, 217 – 220, doi:
325 10.1038/237217a0, 1972.
- Lienert, B. R., Berg, E. and Frazer, L. N.: Hypocenter: an Earthquake Location Method using Centered, Scaled and Adaptively Damped Least Squares, *Bull. Seis. Soc. Am.*, 73(3), 771-783, doi: , 1986)

- Luis, J. F.: Mirone: A multi-purpose tool for exploring grid data. *Computers & Geosciences*, 33(1), 31-41, doi: 10.1016/j.cageo.2006.05.005, 2007.
- 330 Luis, J. F., and Miranda, J. M.: Reevaluation of magnetic chrons in the North Atlantic between 35 N and 47 N: Implications for the formation of the Azores Triple Junction and associated plateau. *J. of Geophys. Res., Solid Earth*, 113(B10), doi :10.1029/2007JB005573, 2008.
- Lynnes, C.S., and Ruff, L.J.: Source process and tectonic implications of the great 1975 North Atlantic earthquake. *Geophys. J. Int.*, 82, 3, 497-510, doi: 10.1111/j.1365-246X.1985.tb05148.x, 1985.
- 335 Menke, W.: *Geophysical data analysis: Discrete inverse theory*. Third Edition, pp 293, ISBN 978-0-12-397160-9. Academic Press, 2012.
- Miranda, J. M., Baptista, M. A., and Omira, R.: On the use of Green's summation for tsunami waveform estimation: a case study. *Geophys. J. Int.*, 199(1), 459-464, doi: 10.1093/gji/ggu266, 2014.
- Moreira, V.S.: *Tsunamis observados em Portugal*. Publicacao GEO,134 (in Portuguese), 1968.
- 340 Ottemöller, L., Voss, P., and Havskov, J.: *Seisan earthquake analysis software for Windows, Solaris, Linux and MacOSX*. Dept. Earth Sci., Univ. Bergen, Bergen, Norway, 2011.
- Rothé, J. P.: The structure of the bed of the Atlantic Ocean. *Eos, Transactions American Geophysical Union*, 32(3), 457-461, doi: 10.1029/TR032i003p00457, 1951.
- Satake, K.: Inversion of tsunami waveforms for the estimation of a fault heterogeneity: Method and numerical experiments. *J. of Physics of the Earth*, 35(3), 241-254, doi:org/10.4294/jpe1952.35.24, 1987.
- 345 Satake, K.: Depth distribution of co-seismic slip along the Nankai Trough, Japan, from joint inversion of geodetic and tsunami data. *J. of Geophys. Res.: Solid Earth (1978–2012)*, 98(B3), 4553-4565, doi: 10.1029/92JB01553, 1993.
- Satake, K., Baba, T., Hirata, K., Iwasaki, S., Kato, T., Koshimura, S., Takenaka, J. and Terada, Y.: Tsunami source of the 2004 off the Kii Peninsula earthquakes inferred from offshore tsunami and coastal tide gauges. *Earth, Planets, and Space*, 57(3), 173-178, doi: 10.1186/BF0335181, 2005.
- 350 Titov, V. V., Gonzalez, F. I., Bernard, E. N., Eble, M. C., Mofjeld, H. O., Newman, J. C., and Venturato, A. J.: Real-time tsunami forecasting: Challenges and solutions. In *Developing Tsunami-Resilient Communities*, 41-58, Springer Netherlands, doi: 10.1007/1-4020-3607-8_3, 2005.
- 355 Tsushima, H., Hino, R., Fujimoto, H., Tanioka, Y. and Imamura, F.: Near- field tsunami forecasting from cabled ocean bottom pressure data. *J. of Geophys. Res.: Solid Earth (1978–2012)*, 114(B6), doi:10.1029/2008JB005988, 2009.
- Udias, A., Arroyo, A. L., and Mezcuá, J.: Seismotectonic of the Azores-Alboran region. *Tectonophysics*, 31(3), 259-289, doi:10.1016/0040-1951(76)90121-9, 1986.
- 360 Wu, T. R., and Ho, T. C.: High resolution tsunami inversion for 2010 Chile earthquake. *Nat. Hazards and Earth Syst. Sci.*, 11(12), 3251-3261, doi:10.5194/nhess-11-3251-2011, 2011.

Yasuda, T., and Mase, H.: Real-time tsunami prediction by inversion method using offshore observed GPS buoy data: nankaido. *J. of Waterway, Port, Coastal, and Ocean Eng.*, 139(3), 221-231, doi:10.1061/(ASCE)WW.1943-5460.0000159, 2012.

365

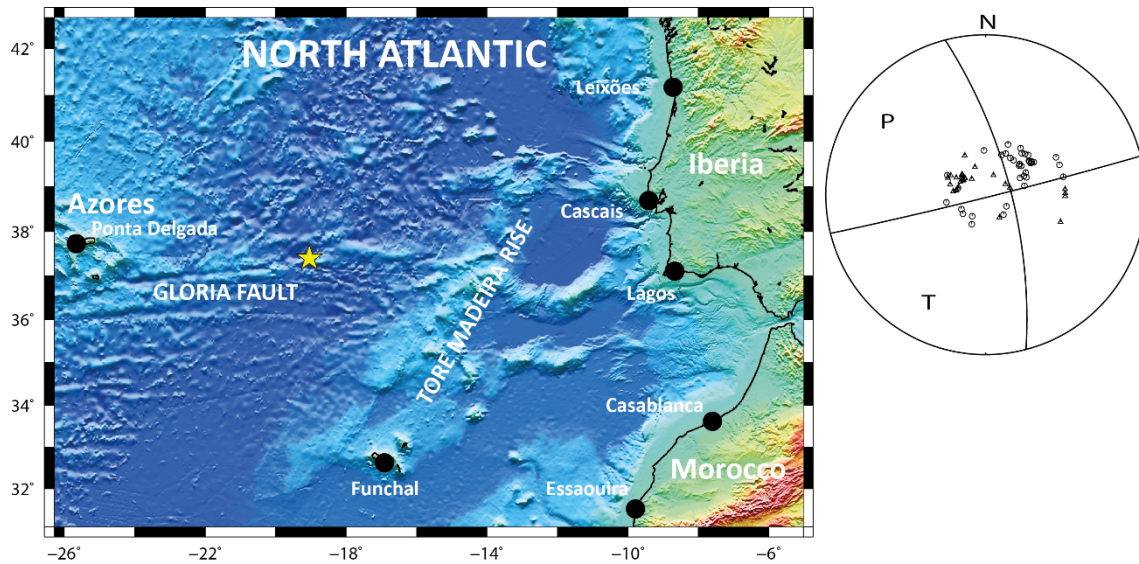
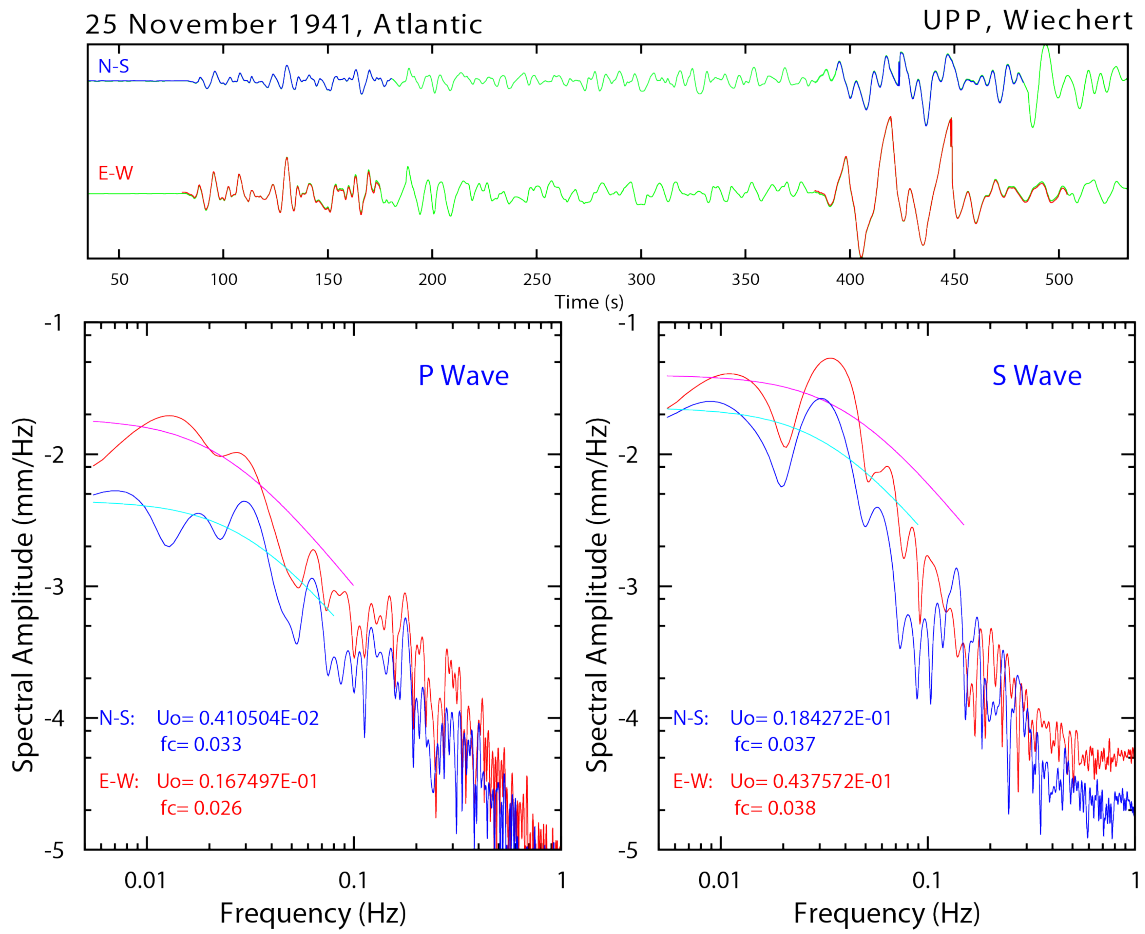


Figure 1: General overview of the North East Atlantic at the latitude of Iberia and focal mechanism of the earthquake. The yellow star represents the epicenter of the earthquake. Black dots show the location of the tide stations.



380

Figure 2: (top) digitized seismograms corresponding to the N-S and E-W components of the 1941 Atlantic earthquake as recorded by the Wiechert seismograph at Uppsala (UPP). (Bottom left) Ground motion spectra of the P-waves, as marked at the top figure (blue and red, respectively), recorded at UPP and the corresponding fit to the Brune's Model. (Bottom right) Ground motion spectra of the S-waves, as marked at the top figure

385

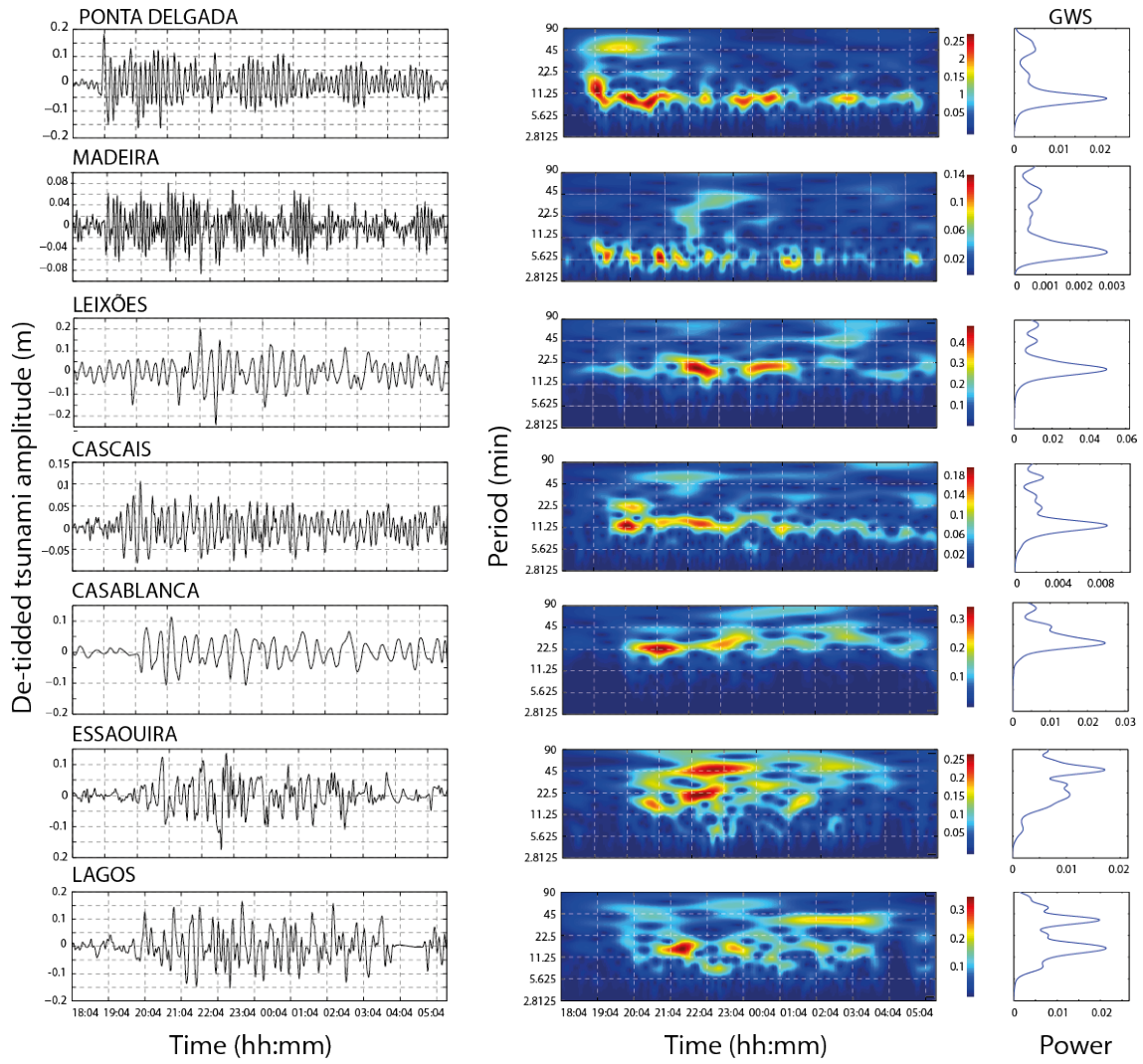


Figure 3 For each station: Left: Tsunami signals (de-tided and filtered record), Middle: wavelet amplitude spectrum and Right: global wavelet spectrum (GWS) Initial time 18.04 hours is the time of the earthquake.

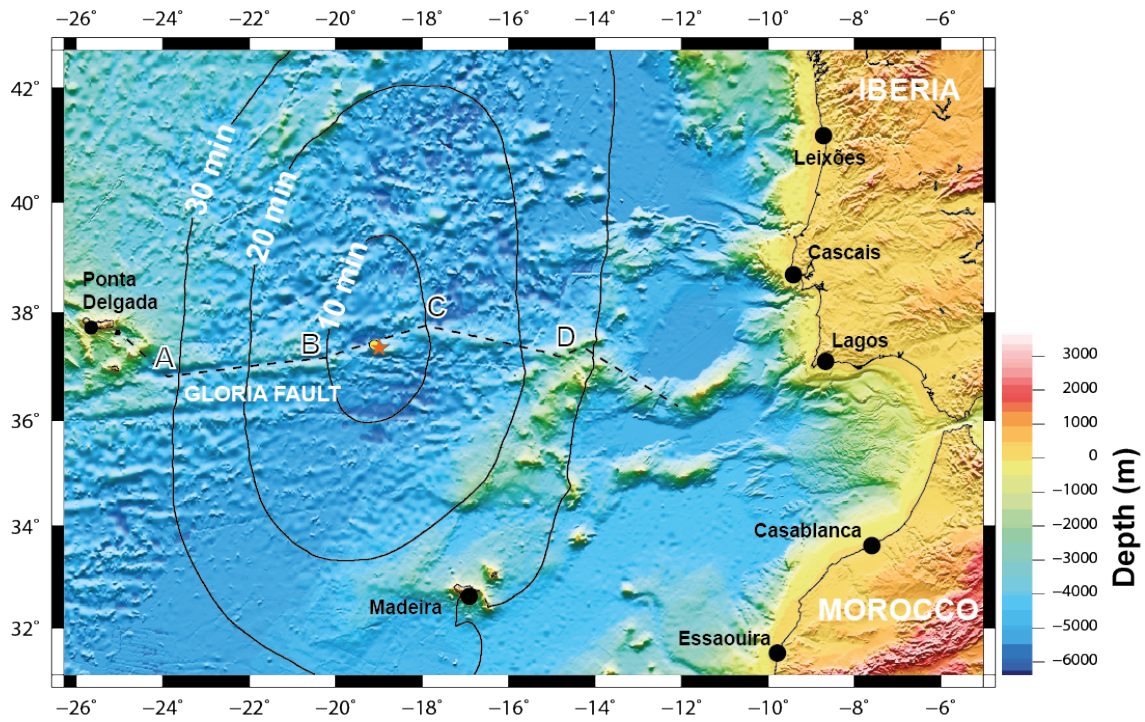


Figure 4: Tsunami source location given by BRT. Red star represents the minimum of the backward ray tracing misfit (~ 7 min) at -19°E , 37.35°N less than 10 km away to the SE of the seismic epicentre -19.038°E , 37.405°N (yellow circle). Black dots represent the tide stations. Segments AB and CD follow the small circle of the Eurasia Nubia rotation pole; segment BC makes an angle of approximately 12° with the small circle of Nuvel 1A.

395

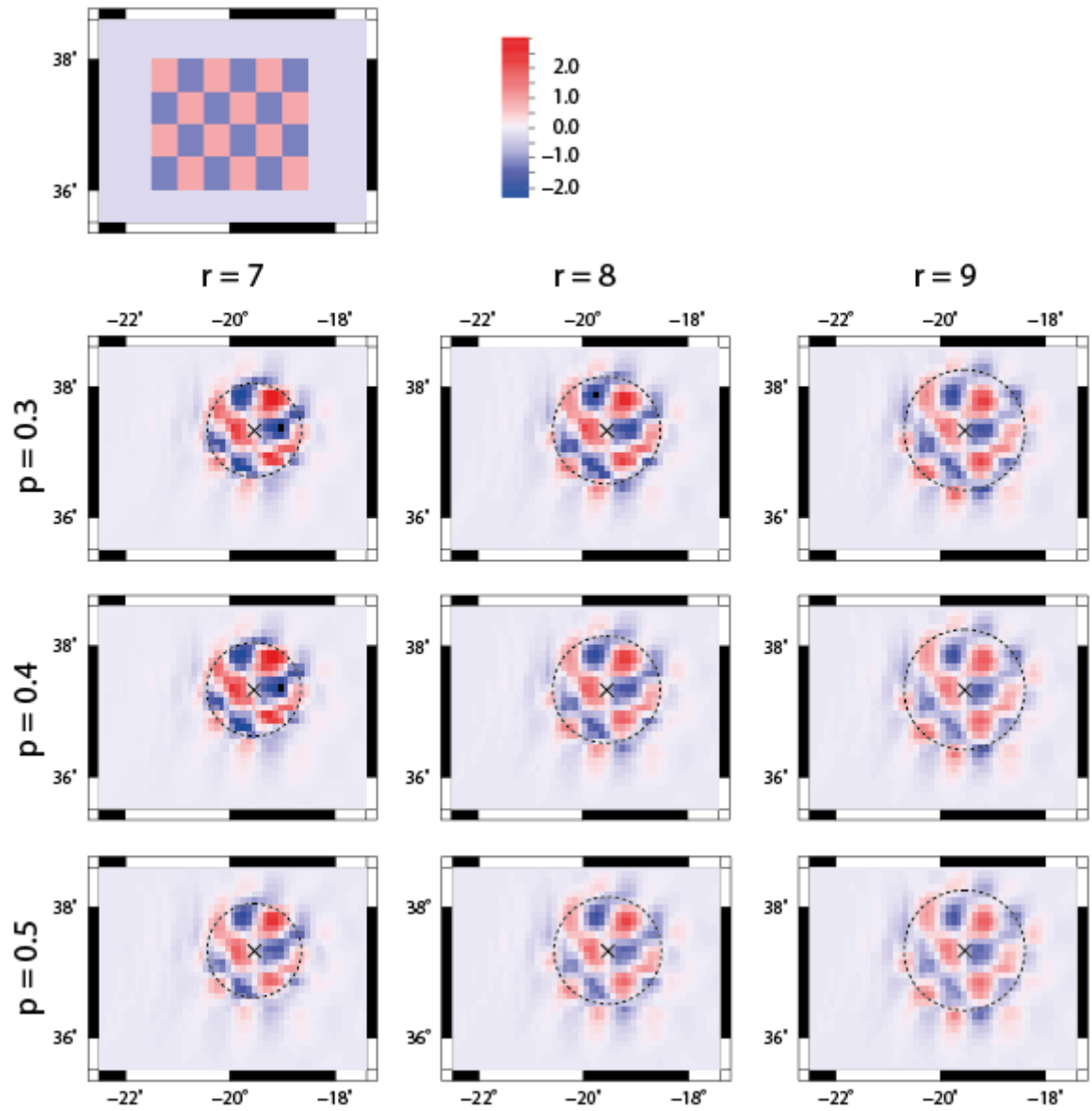
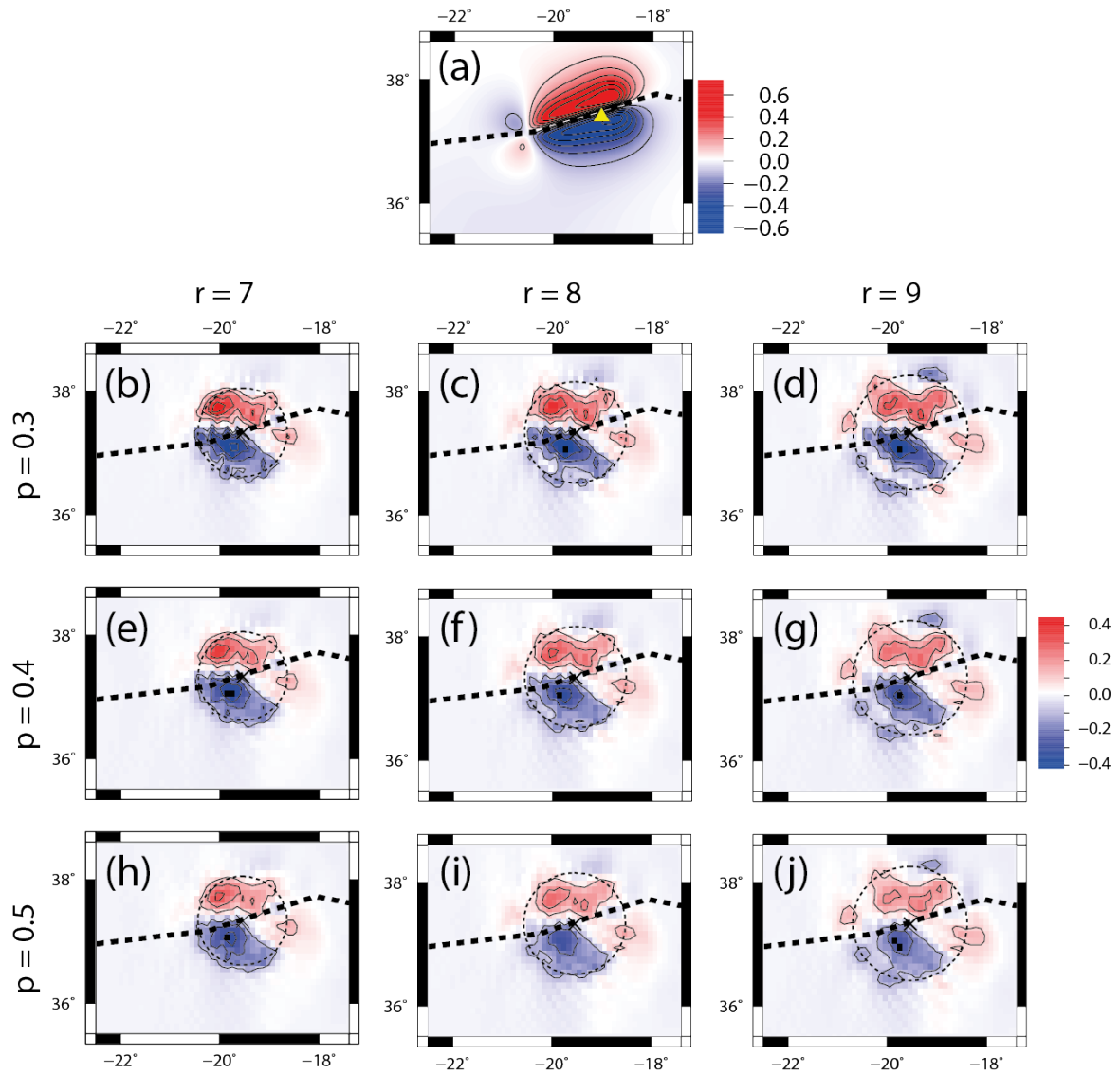
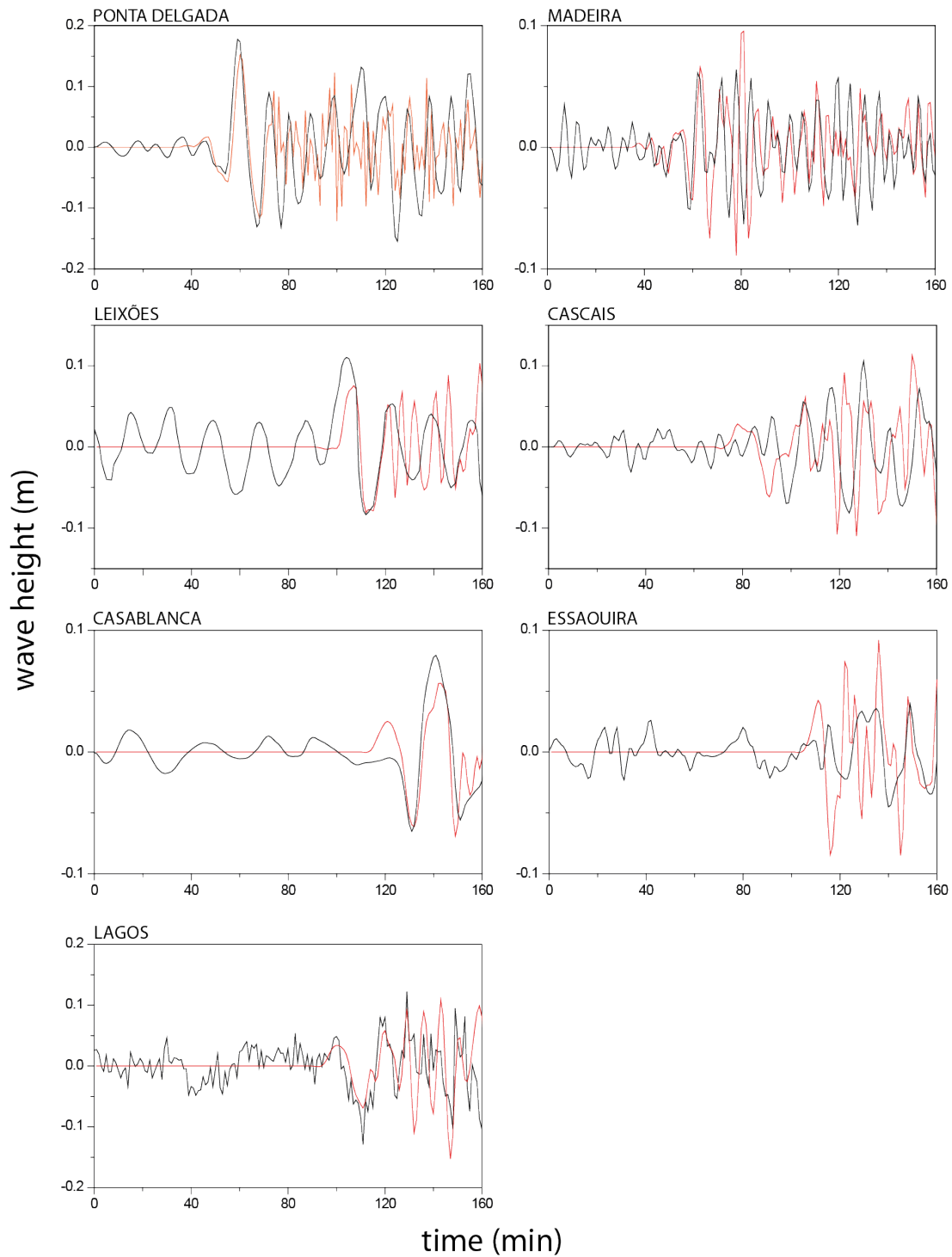


Figure 5: Chessboard test of the inversion approach. The source has alternating +1m/-1m displacements and the synthetic waveforms computed with a shallow water code to the locations that correspond to our tide gauge network. Inversion results for different values of r_{max} (equation 4) and p (equation 5) are depicted.

400



405 **Figure 6:** (a) Co-seismic deformation using the focal mechanism parameters proposed in this study: $L=170$ km, $W=45$ km; Strike= 255° , Rake= 161° , Dip= 88° , slip= 8 m, yellow triangle depicts epicenter; (b)-(j) Initial displacement field of the 1941 Gloria Fault tsunami, obtained from waveform inversion for different values of r and p parameters, dashed line sketches the approximate location of the plate boundary.



410 **Figure 7:** Comparison between observed and synthetic waveforms. The solution shown corresponds to $r=8$ $p=03$. Red Line depicts the synthetic waveform. Black line depicts the observed waveform. Time zero is the time of the earthquake. Time 0 corresponds to the time of the earthquake, that is 18:03:54 of 25.11.1941.

415

Station	Longitude (°E)	Latitude (°N)	Depth (m)	Max. Amplitude (m)	Tsunami Travel Time (minutes)
Ponta Delgada	-25.65	37.73	49.4	0.20	53.0
Madeira	-16.91	32.63	246.9	0.08	55.0
Leixões	-8.71	41.17	10.1	0.20	94.0
Cascais	-9.41	38.69	11.5	0.11	92.0
Casablanca	-7.59	33.62	13.0	0.09	120.0
Essaouira	-9.78	31.51	9.2	0.12	110.0
Lagos	-8.66	37.10	7.8	0.12	107.0

Table 1. POIs of the 1941 tsunami used in this study. Longitude, Latitude and Depth refer to the Point of Interest. POIs are named after the closest tide station.